-RESEARCH PAPER-

International Journal of Mining and Geo-Engineering

IJMGE

IJMGE 59-3 (2025) 273-279

DOI: 10.22059/IJMGE.2025.392402.595229

Comparing the effectiveness of some modern boundary determination methods in interpreting the geology structures of the Tuan Giao area

Hue Bui Thi [a, *] and Thu Thi Nguyen [a]

[a] *University of Economics – Technology for Industries, 456 Minh Khai, Hai Ba Trung, Hanoi, Vietnam.*

Article History:

Received: 20 March 2025.
Revised: 31 May 2025.
Accepted: 27 July 2025.

ABSTRACT

Accurate horizontal boundary definition is essential in geophysical exploration, as it helps delineate subsurface formations and understand tectonic activities. Traditional boundary determination methods often face challenges in resolution and accuracy, necessitating the development of improved techniques. Recently, a range of edge detection techniques has been developed based on derivatives of the field. This study compares the performance of several recently developed edge identification methods, including improvised logistics of the total horizontal gradient, improvised tilt angle of the horizontal gradient, enhanced version of the horizontal tilt angle, the total horizontal gradient of ImpTDX, Gompertz function, and improved edge detector. These methods are evaluated using synthetic models and Bouguer gravity data from the Tuan Giao area, Vietnam. The results showed that the regional structures tend mainly in the NW-SE direction, and some structures in the NE-SW direction.

Keywords: *Edge detections, Gravity anomaly, Structural map, Tuan Giao.*

1. Introduction

Gravity anomalies reveal the spatial distribution of subsurface masses with varying densities. They also provide essential information about faults and tectonic plate boundaries, facilitating the exploration of mineral resources. Various edge detection techniques have been developed to interpret gravity anomalies effectively. These methods enhance the discovery of geological structures by highlighting sharp contrasts in subsurface density variations. Traditional methods, such as the total horizontal gradient (THG) [1], the analytic signal (AS) [2], and the tilt angle (TA) [3], have been widely used in interpreting potential field data. However, these methods often face limitations in resolution and accuracy, especially in complex geological settings [4-6]. To address these issues, boundary detection techniques have been developed. Cooper and Cowan [7] proposed a modified version of the tilt angle method, known as the horizontal tilt angle (TDX).

Ferreira et al. [8] introduced a novel approach called the tilt angle of the total horizontal gradient (TTHG). Cooper [9] introduced the tilt angle of the analytic signal (TAS), based on the total horizontal gradient of the analytic signal amplitude. Chen et al. [10] developed an improved theta map (ITM) method to enhance the resolution of lateral boundaries. Pham et al. [4] introduced another boundary detection technique, referred to as the improved logistic function (IL) method. Melouah and Pham [11] proposed the improved logistic total horizontal gradient (ILTHG) method. Pham [12] suggested another method called the edge detector (ED), which uses the Heaviside step function of the vertical derivative.

Prasad et al. [13] introduced the ImpTTHG method, a boundary detection technique designed to enhance accuracy and resolution. Ibraheem et al. [14] simultaneously introduced the improved horizontal tilt angle (ImpTDX) and the total horizontal gradient of ImpTDX (THG_impTDX). The Gompertz function (GF) is recommended by Alvandi and Ardestani [15] for balancing different amplitude anomalies. Pham [16] introduced the improved edge detection (IED) method. In addition, numerous other approaches have been developed to identify geological structures more accurately and with higher resolution than traditional filters.

These methods include the Nth-order tilt derivative (NTilt) [17]; the total horizontal derivative of the Nth-order tilt derivative (THDR_NTilt) [18]; the logistic function of the total horizontal gradient (LTHG) [19]; Kuwahara and Gaussian filters [20]; the balanced horizontal gradient (BHG) filter and the enhanced total gradient (ETG) [21, 22]; the Hyperbolic domain edge detection filter (GD_T), Hyperbolic domain filter (GD_H), and the total horizontal derivative (THD) in conjunction with the Rootsig activation function (RTHD) [23, 24]; the modified horizontal gradient amplitude method (MHGA) and the hyperbolic tangent of the horizontal gradient amplitudes (HTHG) [25, 26]; the enhanced dip angle map using Kuwahara and Gaussian filters [27]; and a combination of Euler deconvolution and a total horizontal gradient-based edge detector (ED-THGED) [28].

The Tuan Giao area is located in North Vietnam, along major fault systems. The area experiences frequent tectonic movements and earthquakes [29]. Additionally, the region possesses significant mineral potential, including iron, manganese, rare metals, and magmatic rock formations that may contain economically valuable mineral deposits [19, 30]. These geological and mineral features have attracted extensive scientific research, particularly in the fields of geology, geophysics, and seismology.

In this study, the effectiveness of the ILTHG, ImpTTHG, ImpTDX, THG_impTDX, GF, and IED methods was evaluated through a synthetic gravity model. Subsequently, these techniques were applied to Bouguer gravity anomaly data from the Tuan Giao area to map the complex geological structures of the region.

* Corresponding author: *E-mail address:* bthue@uneti.edu.vn (H. Bui Thi).

2. Method

A commonly used boundary detection technique to date is the total horizontal gradient method. This method was proposed by Cordell and Grauch [1] and is expressed by the following formula:

$$\mathrm{THG} = \sqrt{\left(\frac{\partial f}{\partial x}\right)^2 + \left(\frac{\partial f}{\partial y}\right)^2} \tag{1}$$

where $\frac{\partial f}{\partial x}$ and $\frac{\partial f}{\partial y}$ are the horizontal derivatives of potential field data f.

Cooper and Cowan [7] introduced the horizontal tilt angle (TDX), which is defined as:

$$\mathrm{TDX} = \tan^{-1}\left(\frac{\mathrm{THG}}{\left|\frac{\partial f}{\partial z}\right|}\right) \tag{2}$$

where $\frac{\partial f}{\partial z}$ is the vertical derivative of potential field data f.

Melouah and Pham [11] proposed the improved logistic total horizontal gradient (ILTHG) method. This method can provide high-resolution results and balance edge detection at different depths. The ILTHG function is calculated as:

$$\mathrm{ILTHG} = \left[1 + \exp\left(-\frac{\frac{\partial \mathrm{ITHG}}{\partial z}}{\sqrt{\left(\frac{\partial \mathrm{ITHG}}{\partial x}\right)^2 + \left(\frac{\partial \mathrm{ITHG}}{\partial y}\right)^2}}\right)\right]^{-\alpha} \tag{3}$$

where ITHG is calculated using the following expression:

$$\mathrm{ITHG} = \sqrt{\left(\frac{\partial^2 f}{\partial z\,\partial x}\right)^2 + \left(\frac{\partial^2 f}{\partial z\,\partial y}\right)^2} \tag{4}$$

and α is a positive constant, $\alpha = [2, 5]$ gives the best results. Here, we used $\alpha = 5$, as recommended by Melouah and Pham [11].

Prasad et al. [13] proposed the improvised TTHG (ImpTTHG) method, which enhances edge detection by utilizing the first-order derivatives of TTHG. ImpTTHG is defined as follows:

$$\mathrm{ImpTTHG} = \tanh\left(\frac{\partial \mathrm{TTHG}}{\partial z} + \frac{\mathrm{TTHG} - 4\sqrt{\left(\frac{\partial \mathrm{TTHG}}{\partial x}\right)^2 + \left(\frac{\partial \mathrm{TTHG}}{\partial y}\right)^2}}{\left|\mathrm{TTHG} - 2\sqrt{\left(\frac{\partial \mathrm{TTHG}}{\partial x}\right)^2 + \left(\frac{\partial \mathrm{TTHG}}{\partial y}\right)^2}\right|}\right) \tag{5}$$

where TTHG is given by:

$$\mathrm{TTHG} = \tan^{-1}\left(\frac{\left(\frac{\partial \mathrm{THG}}{\partial z}\right)^2}{\sqrt{\left(\frac{\partial \mathrm{THG}}{\partial x}\right)^2 + \left(\frac{\partial \mathrm{THG}}{\partial y}\right)^2}}\right) \tag{6}$$

Ibraheem et al. [14] proposed two filters: ImpTDX and THG_impTDX. These methods enhance edge detection at varying depths. The formulas used to calculate these methods are given as follows:

$$\mathrm{ImpTDX} = \tanh\left(\frac{-\mathrm{M}\left(\frac{\partial^2 f}{\partial x^2} + \frac{\partial^2 f}{\partial y^2}\right)}{\sqrt{\left(\frac{\partial \mathrm{TDX}}{\partial x}\right)^2 + \left(\frac{\partial \mathrm{TDX}}{\partial y}\right)^2}}\right) \tag{7}$$

and

$$\mathrm{THG\_impTDX} = \sqrt{\left(\frac{\partial \mathrm{ImpTDX}}{\partial x}\right)^2 + \left(\frac{\partial \mathrm{ImpTDX}}{\partial y}\right)^2} \tag{8}$$

where M is the average value of the gravity anomaly in the study area.

Alvandi and Ardestani [15] utilized the Gompertz function to improve resolution and balance the horizontal boundaries. It is calculated as follows:

$$\mathrm{GF} = \exp\left\{-\mathrm{k} \times \exp\left[-\frac{\frac{\partial \mathrm{ITHG}}{\partial z}}{\sqrt{\left(\frac{\partial \mathrm{ITHG}}{\partial x}\right)^2 + \left(\frac{\partial \mathrm{ITHG}}{\partial y}\right)^2}} + 1\right]\right\} \tag{9}$$

and ITHG was:

$$\mathrm{ITHG} = \frac{\mathrm{THG}^{\mathrm{k}}}{2 + \sqrt{[\mathrm{H_x(THG)}]^2 + [\mathrm{H_y(THG)}]^2 + \mathrm{THG}^2}} \tag{10}$$

with k is a parameter determined by the interpreter. Tests by Alvandi and Ardestani [15] showed that when $\mathrm{k} = 1$, GF yields sharp signals that maintain their sharpness until $\mathrm{k} = 10$, but the outlined edge is unreliable and faulty if $\mathrm{k} > 4$. Therefore, we can obtain the best results with $\mathrm{k} = [1, 4]$. In this study, we used k = 1 as suggested by Alvandi and Ardestani [15].

Pham [16] introduced the IED method, which is based on the Heaviside step function of the Laplacian. This method is calculated as:

$$\mathrm{IED} = \sqrt{\left(\frac{\partial \mathrm{HL}}{\partial x}\right)^2 + \left(\frac{\partial \mathrm{HL}}{\partial y}\right)^2} \tag{11}$$

where HL is given by:

$$\mathrm{HL} = \mathrm{H}\left(\frac{\partial^2 f}{\partial x^2} + \frac{\partial^2 f}{\partial y^2}\right) = \begin{cases} 0, & \frac{\partial^2 f}{\partial x^2} + \frac{\partial^2 f}{\partial y^2} < 0 \\ \frac{1}{2}, & \frac{\partial^2 f}{\partial x^2} + \frac{\partial^2 f}{\partial y^2} = 0 \\ 1, & \frac{\partial^2 f}{\partial x^2} + \frac{\partial^2 f}{\partial y^2} > 0 \end{cases} \tag{12}$$

3. Synthetic data

The effectiveness of ILTHG, ImpTTHG, ImpTDX, THG_impTDX, GF, and IED methods was tested on a synthetic gravity model. The detailed parameters are presented in Table 1. To assess the effect of depth on these methods, a model was designed with five prisms at varying depths: two prisms (A and B) having the same location but differing in size and depth, two prisms (C and D) having the same size but differing in depth, and a thin prism (E). Figure 1a depicts the plan view, while Figure 1b shows the three-dimensional representation of the model. The evaluation was conducted under two scenarios: a gravity anomaly without noise and a noisy gravity anomaly after an upward continuation to 0.5km. Figure 1c displays the gravity anomaly without noise computed using the space domain method [31]. Figure 2 illustrates the results of applying the filters to the noise-free gravity anomaly. We used the rainbow which is the most widely used color map in the geophysical community to visually represent the intensity of signals. Here, the large amplitudes related to the edges are shown in red in the ILTHG, ImpTTHG, THG_impTDX, GF, and IED maps. Figures 2a and 2b describe the results of the ILTHG with $\alpha = 5$ and ImpTTHG methods. The ILTHG method is capable of balancing edges at different depths. The obtained boundaries are displayed clearly and sharply. However, the ILTHG filter created some false signals around deep sources. The ImpTTHG method cannot outline all the edges of body E, and the edges of sources A and B are thick. The results of the ImpTDX with M=900000, THG_impTDX, GF, and IED methods are displayed in Figures 2c, 2d, 2e, and 2f, respectively. These methods can accurately identify edges at different depths with high resolution. The ImpTDX method identifies boundaries by maximum values over causative sources, making it focus on the anomaly source zones. Although the GF method effectively balances signals at different depths with high resolution, the boundaries of deep sources (A, B, C) are thick. The result of the IED method is similar to the THG_impTDX method. In this case, THG_impTDX and IED accurately define the true boundaries with higher resolution than the ILTHG, ImpTTHG, and GF methods.

Table 1. The parameters of the synthetic model.

Parameters/prism ID	A	B	C	D	E
Center Coordinate x (km)	100	100	50	150	100
Center Coordinate y (km)	50	50	130	130	180
Width (km)	115	75	45	45	170
Length (km)	70	25	45	45	15
Depth of top (km)	14	11	7	4	1
Depth of bottom (km)	17	14	9	6	2.5
Density contrast (g/cm3)	0.2	-0.3	0.1	0.3	0.1

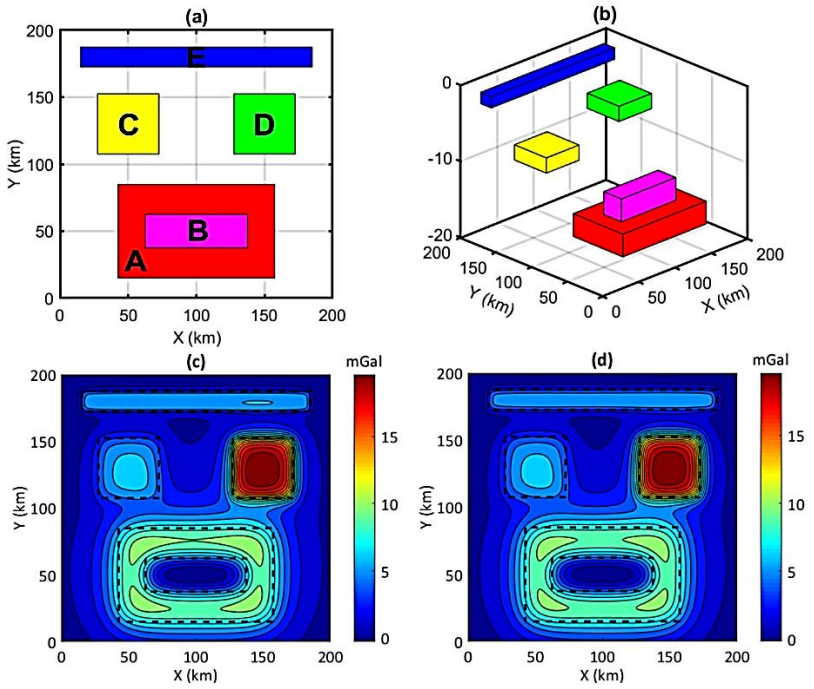

Figure 1. (a) Plan view, (b) 3D view of the synthetic model, (c) gravity anomaly without noise, and (d) noise gravity anomaly after upward continuation of 0.5km.

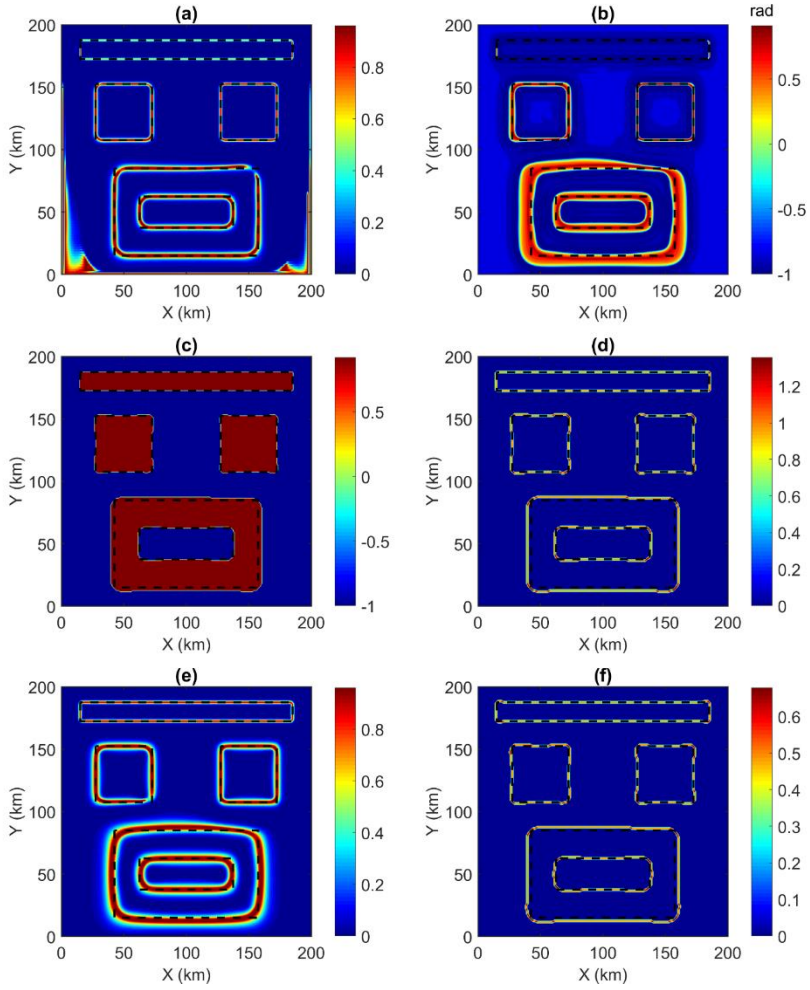

Figure 2. The obtained results of the methods for the gravity anomaly without noise: (a) ILTHG, (b) ImpTTHG, (c) ImpTDX, (d) THG_impTDX, (e) GF, and (f) IED.

Real gravity anomaly data often contain noise that can fade or distort the boundaries. Therefore, selecting appropriate processing methods under noisy conditions is essential for precise geological interpretation. The effectiveness of the ILTHG, ImpTTHG, ImpTDX, THG_impTDX, GF, and IED methods is also evaluated in the noise case. Gaussian random noise with an amplitude of 0.1% of the maximum anomaly amplitude has been added to the synthetic data in Figure 1c. To reduce the effect of noise on the methods, an upward continuation of 0.5 km was performed before applying these methods, as shown in Figure 1d. The results of the ILTHG, ImpTTHG, ImpTDX, and THG_impTDX methods are displayed in Figures 3a, 3b, 3c, and 3d, respectively. It can be observed that all four methods are strongly affected by noise. The ILTHG method cannot obtain clear signals on the boundaries of deep objects (A, B, C).

Unlike the first case, the ImpTTHG method can clarify the structure of the shallow source (E). However, the obtained result is quite noisy. The ImpTDX filter showed anomalous source zones, while the THG_impTDX filter showed the edges of the prisms. These two methods enhanced noise signals around the deep sources (A, B, C). The result of the GF filter (Figure 3e) shows thick edges and is quite noisy. The ILTHG, ImpTTHG, ImpTDX, THG_impTDX, and GF methods all exhibited secondary signals, making it challenging to interpret geological structures. The result of the IED filter (Figure 3f) demonstrated that this method can balance edges with high resolution, almost eliminating noise signals. In this case, the IED filter can extract the best image of the edges.

4. Real gravity data

4.1. Geological and data setting

The Tuan Giao region is a part of northwest Vietnam, at longitudes between 102.98°E and 104.03°E and latitudes from 20.97°N to 22.38°N. This area has a complicated geological structure with many faults tending to the NW-SE direction, seismic activities, and high mineral potential [29]. Figure 4a illustrates the study area and some adjacent areas [30, 32]. It lies along the Dien Bien-Lai Chau fault zone and the Son La fault, parts of the Red River shear zone. It has caused significant earthquakes, such as the magnitudes M=6.8 (1935) and M=6.7 (1983) [29]. Gravity and magnetic anomaly data show that magmatic activities and fault-controlled hydrothermal systems are associated with iron, manganese, and rare metal mineralization [19, 33]. Given the geological complexity and seismic risk, the area remains a subject of ongoing investigation and continuous monitoring.

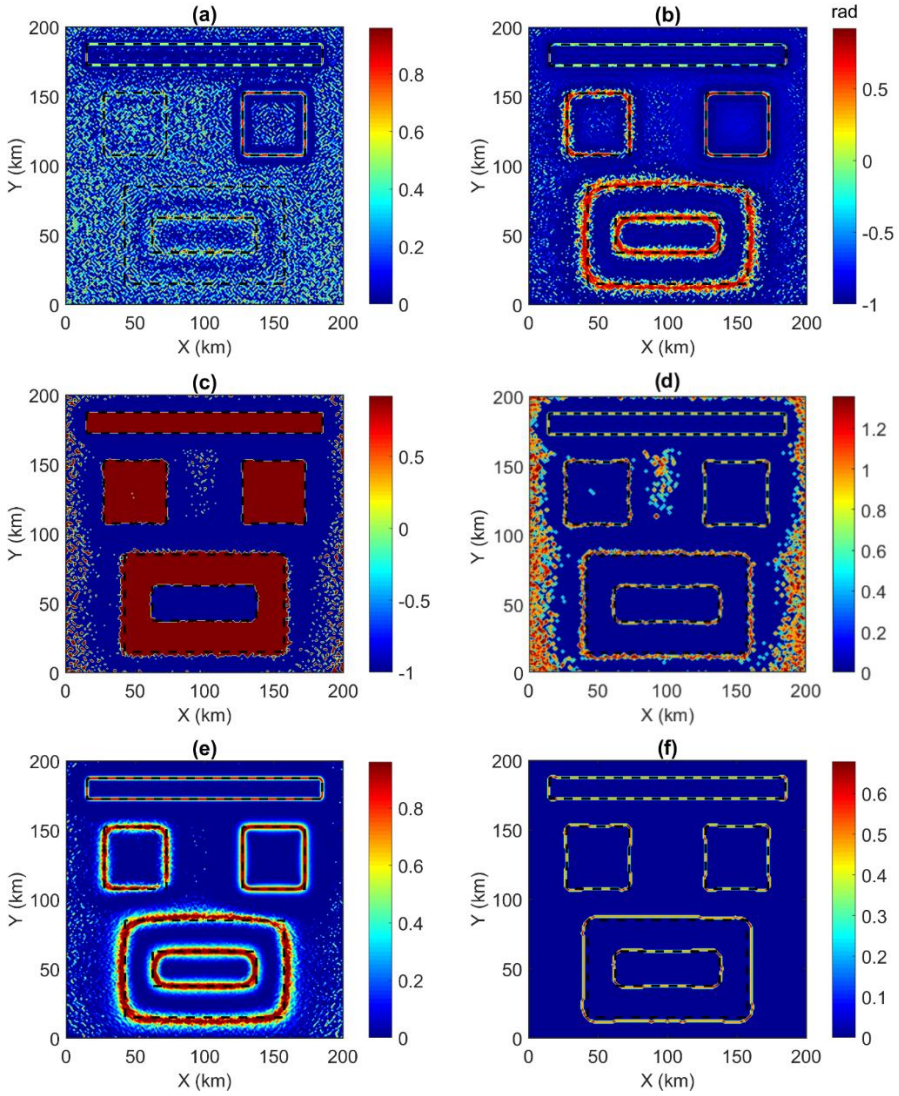

Figure 3. The obtained results of the methods for the noise gravity anomaly after upward continuation of 0.5km: (a) ILTHG, (b) ImpTTHG, (c) ImpTDX, (d) THG_impTDX, (e) GF, and (f) IED.

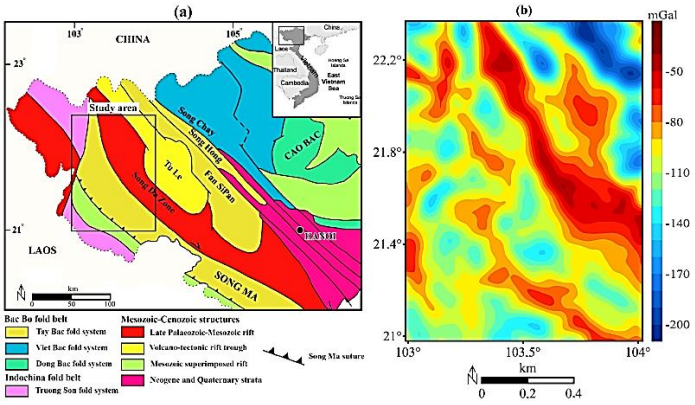

Figure 4. (a) Geology map of the study area and around regions [30, 32], and (b) the Bouguer gravity anomaly map of the study area.

Bouguer gravity data for the study area were calculated by Pham [34] based on the latest 1'×1' grid data from the TOPEX mission, including topographic data and satellite-derived free-air gravity data. The Bouguer gravity anomaly map of the study area is displayed in Figure 4b. The gravity anomalies are mainly oriented in the NW-SE direction, which correlates with the geological structure.

4.2. Results

In this scenario, the effectiveness of the boundary determination methods is evaluated based on the interpretation of Bouguer gravity anomaly data from the study area. Figure 5a shows the obtained result using the ILTHG method. The ILTHG filter can equalize different structures simultaneously, but some adjacent ones are connected. In addition, ILTHG is also strongly affected by noise, making it difficult to determine boundaries. The obtained structure map from the ImpTTHG method is illustrated in Figure 5b. The ImpTTHG function presented the boundary anomalies more clearly than ILTHG. However, these structures are discontinuous. Figures 5c, 5d, and 5e describe the obtained structural maps from the ImpTDX, THG_impTDX, and GF methods, respectively. The results demonstrate that these methods are superior to ILTHG and ImpTTHG. The obtained results by the ImpTDX method are shown as red and blue zones, making it difficult to determine the lineament structure. Conversely, the THG_impTDX filter displays clear peaks over the body's edges. ImpTDX and its THG still generated some secondary structures around the causative sources. This leads to false information in interpreting the area's geological structure. Figure 5e shows that the GF function effectively equalized the large and small amplitudes of the anomalies. However, the boundaries created by the causative sources at great depths tend to blur and have thicker edges than their true extent. The obtained structures by the IED technique are described in Figure 5f. IED extracted edges of anomalous sources with the highest resolution without creating false boundaries compared to the ILTHG, ImpTTHG, ImpTDX, THG_impTDX, and GF methods. The IED filter highlighted structures trending NW–SE, with a few in the NE–SW direction.

The IED function shows that the gravity lines correspond to many faults in the region, as presented in Figure 6. The blue gravity lines illustrate the distribution of gravity anomaly boundaries from the IED method. Meanwhile, the black faults represent the major faults in the region, as identified in Figure 4a. These black faults are also used to divide the tectonic zones of the area [29]. It can be observed that the gravity lines in the northwest are related to the Dien Bien fault and the Truong Son fold system. In the northeast, the gravity lines match the boundaries between the Song Da region and the Tu Le basin, as well as the boundary between the Tu Le basin and the Fansipan region. In the southwest, the gravity lines correspond to the boundaries of the Truong Son fold belt and the Song Ma shear zone. The correlation between the gravity lines and the known faults provided crucial information about the tectonic processes, subsurface structure, and geological history in the study area.

The major fault and fold systems strongly influenced the gravity anomalies, which in turn controlled the distribution of geological units and their associated densities. These findings emphasized the critical role of fault and fold structures in shaping the geophysical characteristics and offer valuable insights for future research.

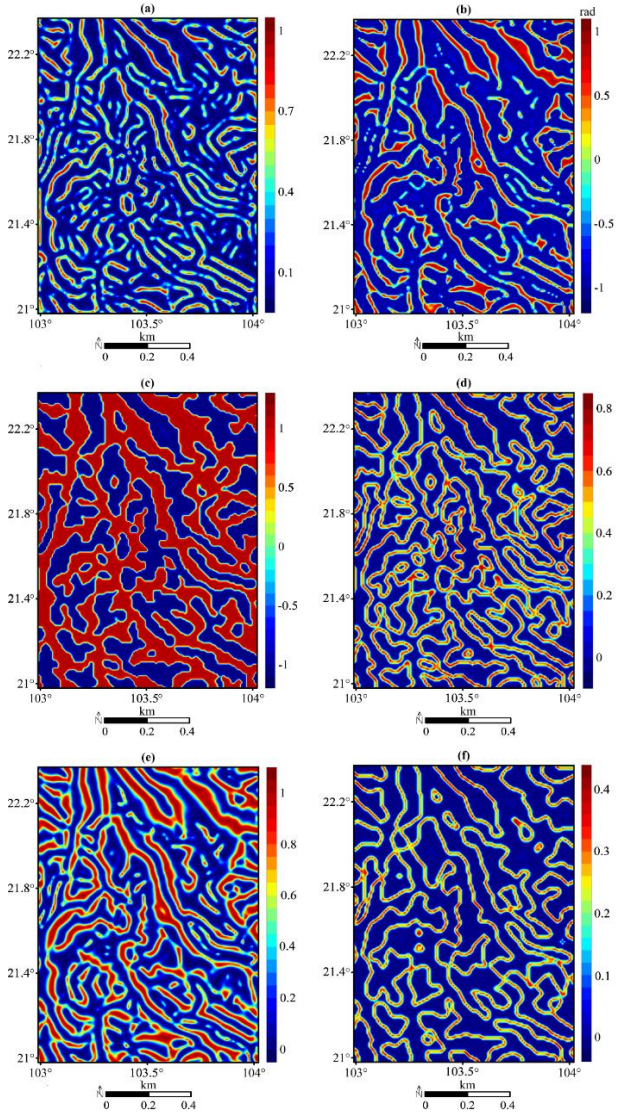

Figure 5. The obtained results of the methods: (a) ILTHG, (b) ImpTTHG, (c) ImpTDX, (d) THG_impTDX, (e) GF, and (f) IED.

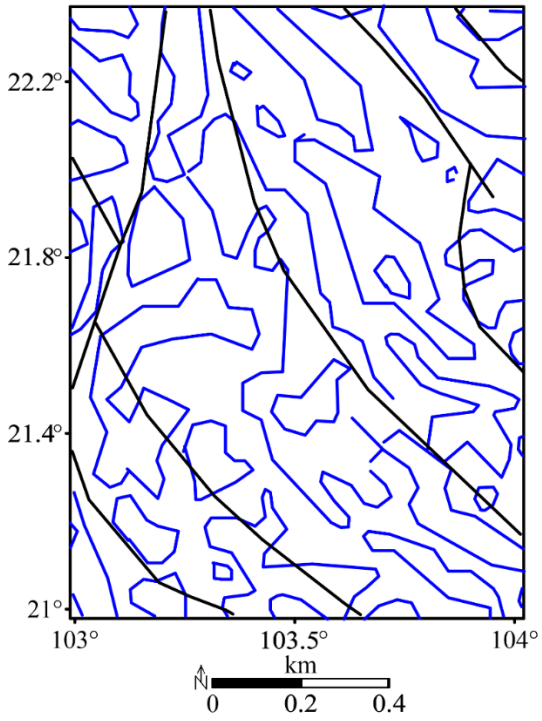

Figure 6. Gravity lineaments (blue lines) of the IED map and faults (black lines).

5. Conclusions

The effectiveness of edge detection techniques, such as the ILTHG, ImpTTHG, ImpTDX, THG_impTDX, GF, and IED methods has been estimated using a synthetic gravity model and real data from the Tuan Giao area, Vietnam. The obtained results showed that the methods can balance the edges of the causative sources located at different depths. However, the ImpTTHG and GF methods create thick edges, while the ILTHG and THG_impTDX methods are more sensitive to noise than the others. The findings also showed that the IED can provide the best results compared to other methods. The obtained boundaries were accurately and clearly delineated without creating false structures. The analysis of the Bouguer gravity anomaly using the IED method reveals that the extracted gravity lineaments correspond well with the known geological structures of the study area. Besides, IED revealed several structures that were not represented on the geological map. Therefore, the IED method can be considered a valuable tool for future studies and more detailed exploration in the study area.

References

[1] Cordell, L., and V.J.S. Grauch. (1985). Mapping basement magnetization zones from aeromagnetic data in the San Juan basin, New Mexico. The utility of regional gravity and magnetic anomaly maps, 16,181–197. https://doi.org/10.1190/1.0931830346.ch16

[2] Roest, W.R.J., J. Verhoef, and M. Pilkington. (1992). Magnetic interpretation using the 3-D analytic signal. Geophysics, 57(1),116–125. https://doi.org/10.1190/1.1443174

[3] Miller, H.G., and V. Singh. (1994). Potential field tilt: A new concept for location of potential field sources. Journal of Applied Geophysics, 32,213–217. https://doi.org/10.1016/0926-9851(94)90022-1

[4] Pham, L.T., T.V. Vu, S. Le-Thi, and P.T. Trinh. (2020). Enhancement of potential field source boundaries using an improved logistic filter. Pure and Applied Geophysics, 177 (11), 5237–5249. https://doi.org/10.1007/s00024-020-02542-9

[5] Pham, L.T., S.P., Oliveira, L.D., Luu, and L.T. Do. (2025). Enhancing potential fields using stable downward continuation and boundary filters: Application to the Central Highlands, Vietnam. Vietnam Journal of Earth Sciences, 47(2), 1-16. https://doi.org/10.15625/2615-9783/22702.

[6] Aprina, P.U., D. Santoso, S. Alawiyah, N. Prasetyo, and K. Ibrahim. (2024). Delineating geological structure utilizing integration of remote sensing and gravity data: a study from Halmahera, North Molucca, Indonesia. Vietnam Journal of Earth Sciences 46 (2), 147–68. https://doi.org/10.15625/2615-9783/20010.

[7] Cooper, G.R.J., and D.R. Cowan. (2006). Enhancing potential field data using filters based on the local phase. Computers & Geosciences, 32(10),1585–1591. https://doi.org/10.1016/j.cageo.2006.02.016

[8] Ferreira, F.J.F., J. de Souza, A. de BeS Bongiolo, and L.G. de Castro. (2013). Enhancement of the total horizontal gradient of magnetic anomalies using the tilt angle. Geophysics, 78(3),J33–J41. https://doi.org/10.1190/geo2011-0441.1

[9] Cooper, G.R.J. (2014). Reducing the dependence of the analytic signal amplitude of aeromagnetic data on the source vector direction. Geophysics, 79, J55–J60. https://doi.org/10.1190/geo2013-0319.1

[10] Chen, A.G., T.F. Zhou, D.J. Liu, and S. Zhang. (2017). Application of an enhanced theta-based filter for potential field edge detection: A case study of the Luzong ore district. Chinese Journal of Geophysics, 60(2),203–218. https://doi.org/10.6038/cjg20170228

[11] Melouah, O., and L.T. Pham. (2021). An improved ILTHG method for edge enhancement of geological structures: Application to gravity data from the Oued Righ valley. Journal of African Earth Sciences, 177,104162. https://doi.org/10.1016/j.jafrearsci.2021.104162

[12] Pham, L.T. (2021). A high-resolution edge detector for interpreting potential field data: A case study from the Witwatersrand basin, South Africa. Journal of African Earth Sciences, 178,104190. https://doi.org/10.1016/j.jafrearsci.2021.104190

[13] Prasad, K.N.D., L.T. Pham, A.P. and Singh. (2022). A novel filter "ImpTAHG" for edge detection and a case study from Cambay Rift Basin, India. Pure and Applied Geophysics, 179(6–7),2351–2364. https://doi.org/10.1007/s00024-022-03059-z

[14] Ibraheem, I.M., B. Tezkan, H. Ghazala, and A.A. Othman. (2023). A new edge enhancement filter for the interpretation of magnetic field data. Pure and Applied Geophysics, 180,2223–2240. https://doi.org/10.1007/s00024-023-03249-3

[15] Alvandi, A., and V.E. Ardestani. (2023). Edge detection of potential field anomalies using the Gompertz function as a high-resolution edge enhancement filter. Bulletin of Geophysics & Oceanography, 64(3),279–300. https://doi.org/10.4430/bgo00420

[16] Pham, L.T. (2024). An improved edge detector for interpreting potential field data. Earth Science Informatics, 17(3),2763–2774. https://doi.org/10.1007/s12145-024-01286-7

[17] Nasuti, Y., and A. Nasuti. (2018). NTilt as an improved enhanced tilt derivative filter for edge detection of potential field anomalies. Geophysical Journal International, 214(1),36–45. https://doi.org/10.1093/gji/ggy117

[18] Nasuti, Y., A. Nasuti, and D. Moghadas. (2019). STDR: A novel approach for enhancing and edge detection of potential field

data. Pure and Applied Geophysics, 176(2),827–841. https://doi.org/10.1007/s00024-018-2016-5

[19] Pham, L.T., E. Oksum, and T.D. Do. (2019). Edge enhancement of potential field data using the logistic function and the total horizontal gradient. Acta Geodaetica et Geophysica, 54(1),143–155. https://doi.org/10.1007/s40328-019-00248-6

[20] Kafadar, Ö. (2022). Applications of the Kuwahara and Gaussian filters on potential field data. Journal of Applied Geophysics, 198,104583. https://doi.org/10.1016/j.jappgeo.2022.104583

[21] Prasad, K.N.D., L.T. Pham, and A.P. Singh. (2022). Structural mapping of potential field sources using BHG filter. Geocarto International, 37(26),11253–11280. https://doi.org/10.1080/10106049.2022.2048903

[22] Prasad, K.N.D., L.T. Pham, A.P. Singh, A.M. Eldosouky, K. Abdelrahman, M.S. Fnais, and D. Gómez-Ortiz. (2022). A novel enhanced total gradient (ETG) for interpretation of magnetic data. Minerals, 12(11),1468. https://doi.org/10.3390/min12111468

[23] Alvandi, A., K. Su, H. Ai, V.E. Ardestani, and C. Lyu. (2023). Enhancement of potential field source boundaries using the hyperbolic domain (Gudermannian function). Minerals, 13(10),1312. https://doi.org/10.3390/min13101312

[24] Alvandi, A., V.E. Ardestani, and S.H. Motavalli-Anbaran. (2024). A novel method for interpreting potential field anomalies using the Rootsig function. International Journal of Mining and Geo-Engineering. https://doi.org/10.22059/ijmge.2024.382962.595198

[25] Ai, H., H. Deniz Toktay, A. Alvandi, R. Pašteka, K. Su, and Q. Liu. (2024). Advancing potential field data analysis: the modified horizontal gradient amplitude method (MHGA). Contributions to Geophysics and Geodesy, 54(2),119–143. https://doi.org/10.31577/congeo.2024.54.2.1

[26] Ai, H., Y.L. Ekinci, A. Alvandi, H. Deniz Tokta, C. Balkaya, and A. Roy. (2024). Detecting edges of geologic sources from gravity or magnetic anomalies through a novel algorithm based on hyperbolic tangent function. Turkish Journal of Earth Sciences, 33(6),684-701. https://doi.org/10.55730/1300-0985.1936

[27] Kafadar, Ö., and E. Oksum. (2024). Enhanced dip angle map using Kuwahara and Gaussian filters: An example from Burdur region. Turkish Journal of Earth Sciences, 33(4),395–406. https://doi.org/10.55730/1300-0985.1919

[28] Pham, L.T., S.P. Oliveira, M. Le-Huy, D.V. Nguyen, T.Q. Nguyen-Dang, T.D. Do, K.V. Tran, T.N. Hong-Duyen, T.N. To-Nhu, and H.Q. Pham. (2024). Reliable Euler deconvolution solutions of gravity data throughout the β-VDR and THGED methods: Application to mineral exploration and geological structural mapping. Vietnam Journal of Earth Sciences, 46(3),432–448. https://doi.org/10.15625/2615-9783/21009

[29] Tuyen, N.H., P.V. Phach, R.B. Shakirov, C.D. Trong, P.N. Hung, and L.D. Anh. (2018). Geoblocks recognition and delineation of the earthquake-prone areas in the Tuan Giao area (Northwest Vietnam). Geotectonics, 52,359–381. https://doi.org/10.1134/S001685211803007X

[30] Koszowska, E., A. Wolska, W. Zuchiewicz, N.Q. Cuong, and Z. Pécskay. (2007). Crustal contamination of Late Neogene basalts in the Dien Bien Phu Basin, NW Vietnam: Some insights from petrological and geochronological studies. Journal of Asian Earth Sciences, 29(1),1–17. https://doi.org/10.1016/j.jseaes.2005.12.003

[31] Rao, D.B., M.J. Prakash, N. Ramesh Babu. (1990). 3-D and 2 1/2-D modeling of gravity anomalies with variable density contrast. Geophysical Prospecting, 38,411–422. https://doi.org/10.1111/j.1365-2478.1990.tb01854.x.

[32] Pham, L.T. (2023). A novel approach for enhancing potential fields: application to aeromagnetic data of the Tuangiao, Vietnam. The European Physical Journal Plus, 138, 1134. https://doi.org/10.1140/epjp/s13360-023-04760-1

[33] Pham, L.T., S.P. Oliveira, C.V.S. Le, N.T. Bui, A.H. Vu, and D.A. Nguyen. (2023). Gravity data enhancement using the exponential transform of the tilt angle of the horizontal gradient. Minerals, 13(12),1539. https://doi.org/10.3390/min13121539

[34] Pham, L.T. (2020). A comparative study on different methods for calculating gravity effect of an uneven layer: Application to computation of Bouguer gravity anomaly in the East Vietnam Sea and adjacent areas. VNU Journal of Science: Mathematics - Physics, 36(3),106–114. https://doi.org/10.25073/2588-1124/vnumap.4515